JOURNAL OF MATERIALS SCIENCE 35 (2000) 1525–1533

Impact properties of glass fibre/impact modifier/polypropylene hybrid composites

W. Y. TAM, T. Y. H. CHEUNG, R. K. Y. Li*
Department of Physics and Materials Science, City University of Hong Kong, Tat Chee Avenue, Kowloon, Hong Kong
E-mail: aprkyl@cityu.edu.hk

The impact properties of glass-fibre/impact-modifier/polypropylene (GF/IM/PP) hybrid composites were characterized using a number of impact test methods. For the IM/PP blends, the impact fracture toughness can be measured using linear elastic fracture mechanics (LEFM) approach. For the GF/IM/PP hybrids, due to their non-compliance with LEFM, the essential work of fracture approach was employed. The impact properties of the IM/PP blends increased with IM concentration, while that of the GF/IM/PP hybrids did not change very much with IM content. It was concluded that cavitation of the PP matrix around the IM particles was the major toughening mechanism in the IM/PP blends. However, in the GF/IM/PP hybrids, the toughening effect due to cavitation was suppressed due to the introduction of short glass fibres (≈15 vol%). It is believed that the local stress in the matrix was relieved by fibre/matrix debonding of the relatively weak fibre/matrix interface. Thus, the presence of the IM particles was rendered insignificant in the GF/IM/PP hybrids.

1. Introduction

Polypropylene (PP) homopolymer is known to suffer from brittle failure at either low temperature or high loading rates. Improvement in the fracture toughness of PP can be achieved by either modifying the crystalline structure [1, 2], or addition of a second phase material. The toughening effect and mechanisms of different second phase materials like stiff fibres (e.g. glass fibres) [3–6], mineral fillers (e.g. calcium carbonate and talc) [7–9], and soft rubbery inclusions (e.g. EPR and EPDM) [10–13] have been well documented. However, the effect of the incorporation of both rigid and rubbery inclusions is not fully understood [14, 15].

This work concerns with the addition of an impact modifier (IM) on the impact behaviour of short glass fibre reinforced polypropylene (GF/PP). Particular attention will be paid to the fracture resistance of the IM/PP blends and IM/GF/PP hybrids measured using different impact testing methods.

2. Experimental method

2.1. Materials and sample preparation

PP homopolymer (Pro-fax 6331), PP/PE copolymer (Hi-fax RA061), and short glass fibre reinforced PP (Hi-glass PF062 series) in pellet form were supplied by Montell Hong Kong Ltd. A summary of the materials used in this work to prepare the blends and hybrids is shown in Table I. In the preparation of the various blends and hybrids, the pellets were mixed in the appropriate ratio so as to achieved the required impact modifier, glass fibre, and PP homopolymer concentration. The mixed pellets were subsequently compounded using a Brabender twin screw compounder at a barrel temperature of 220 °C.

A summary of the composition of the blends and hybrids as well as their designation is given in Table II. The volume fraction for each constituent phase V_i (where i = PP, IM or GF) are related to the weight fraction W_i by Equation 1:

$$V_i = \frac{\dfrac{W_i}{\rho_i}}{\dfrac{W_{PP}}{\rho_{PP}} + \dfrac{W_{IM}}{\rho_{IM}} + \dfrac{W_{GF}}{\rho_{GF}}} \quad (1)$$

where the densities (ρ_i) for PP, IM and glass fibre are taken as 0.90, 0.88 and 2.69 g/cm^3 respectively. In the hybrids, the glass fibre volume fraction was kept to be about 15%.

The blended extrudates were pelletised and injection moulded into plaques with dimensions 6 × 80 × 150 mm^3 using a Chen Hsong Mark II-C injection moulding machine. The mould cavity was end-gated with a film gate. Due to the skin-core structure and the fibre orientation effect [3], a complicated microstructure is expected for the hybrid samples. It is therefore important to control the position and orientation of the specimens. In this work, all specimens were cut with their long dimension parallel to the long dimension of the injection moulded plaques, and the crack orientation

* Author to whom all correspondence should be addressed.

TABLE I Summary of materials used to prepare the blends and hybrids

Material code	Description	Tensile modulus	Tensile strength
Pro-fax 6331	PP homopolymer	2.0 GPa	36 MPa
Hi-fax RA 061	PP/PE copolymer	—	—
Hi-glass PF062-2	20 wt% glass fibre reinforced PP	4.6 GPa	63 MPa
Hi-glass PF062-3	30 wt% glass fibre reinforced PP	6.4 GPa	70 MPa
Hi-glass PF062-4	40 wt% glass fibre reinforced PP	8.6 GPa	79 MPa
Hi-glass PF062-5	50 wt% glass fibre reinforced PP	11.8 GPa	83 MPa

TABLE II Compositions of the IM/PP blends and IM/GF/PP hybrids used in this work

Designation of the blends and hybrids used in this work	Volume % of PP homopolymer	Volume % of impact modifier	Volume % of glass fibres
PP	100	0	0
9IM	91.0	9.0	0
17IM	83.4	16.6	0
30IM	70.8	29.2	0
0GF	84.8	0	15.2
9GF	75.8	9.0	15.2
17GF	68.2	16.6	15.2
30GF	55.6	29.2	15.2

of the specimens was all perpendicular to the melt flow direction (MFD). Before impact specimens were cut from the moulded plaques, 5 mm of materials were removed from both edges. For each type of impact tests, specimens were cut from fixed positions in order to maintain the same microstructural details around the crack tip regions.

2.2. Fibre length distribution

For the hybrid samples, the IM and PP phases were burnt off in an oven. The remaining short glass fibre bundles were dispersed in water with the aid of an ultrasonic bath. The dispersed fibres were collected and dried on a filter paper. The lengths of 1000 fibres for each type of hybrids were measured using an image analyzer.

2.3. Impact testings

Different impact test methods were used to characterize the impact behaviour of the blends and hybrids. All the tests were conducted at a temperature of 20 °C.

2.3.1. Notched and un-notched Charpy impact test

Notched and un-notched Charpy impact tests were carried out according to ASTM D256-84 using a Ceast pendulum impact tester. The notch was opened using a Ceast v-notch cutter. Five tests were performed for each composition and the average is reported.

2.3.2. Impact fracture toughness

Measurement of the impact fracture toughness for both blends and hybrids were carried out using the single edge notched bend (SENB) specimen geometry (Fig. 1a). Dimensions of the SENB bars are $6 \times 75 \times 13$ mm. The samples were simply supported with a span (S) of 52 mm (span/width = 4). The sharp notch in the sample was introduced by first sawing a slot, followed by tapping with a fresh razor blade. The crack length a was measured from the fractured sample using a travelling microscope. The ligament (l) is defined as $l = W - a$. An instrumented Fractovis drop-weight impact tester (Ceast) was used to obtain the impact force-time curves and impact fracture energy. In order to reduce the magnitude of the secondary oscillations that were found on the impact force-time curves, a striker velocity of 2 m/s was employed.

In this work, it has been observed that different techniques have to be employed for the measurement of the impact fracture toughness for the blends and hybrids.

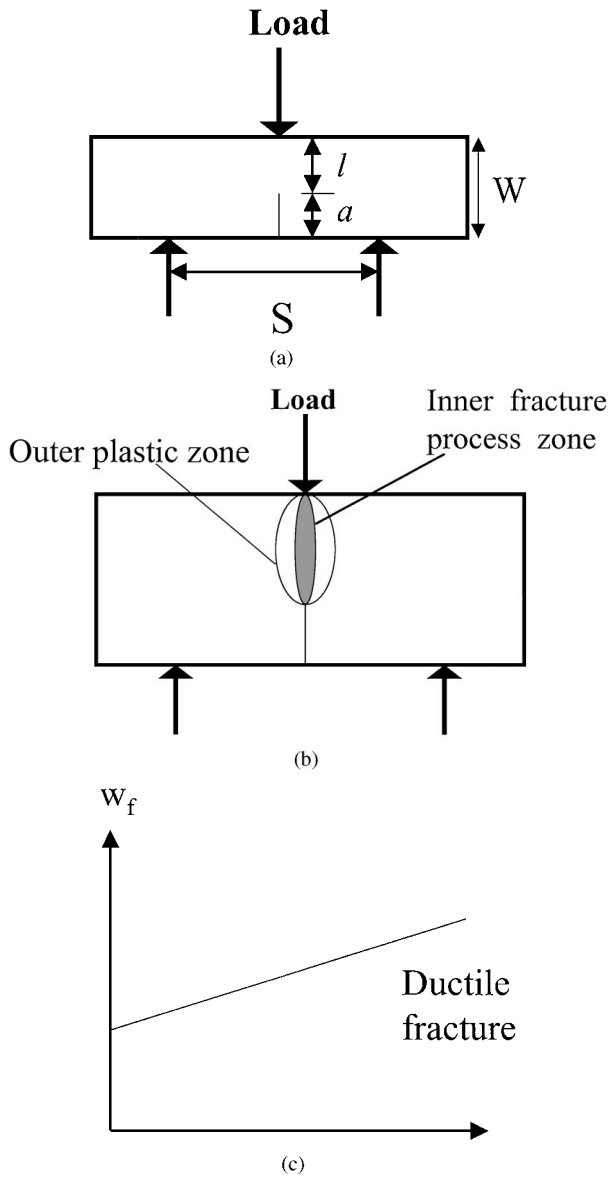

Figure 1 (a) Schematic diagrams showing: SENB specimen geometry; (b) inner fracture process zone and outer plastic zone for SENB specimens; and (c) relationship between the total specific fracture work (w_p) and ligament (l) for ductile fracture.

For the blends, the critical strain energy release rate G_C values were calculated from the equation [16]:

$$U = G_C BW\phi + E_k \quad (1)$$

where U is the impact fracture energy, B is the sample thickness, W is the sample width, E_k is the kinetic energy loss and ϕ is the calibration factor which depends on the ratio a/W. If the linear elastic fracture mechanics (LEFM) conditions were satisfied, a plot of U against $BW\phi$ would yield a straight line with G_C being the gradient.

If, however, the materials do not confirm to LEFM (i.e. a straight line relationship cannot be obtained from the U against $BW\phi$ plot even after a crack tip plastic zone correction were made [13]), the essential work theory [17, 18] were applied. The essential work of fracture concept can be explained as follows. For the fracture of a pre-cracked specimen, the total fracture work (W_f) can be written as:

$$W_f = W_e + W_p \quad (2)$$

where W_e is the essential work of fracture, which is related to the energy of the formation of the fractured surfaces in the inner fracture process zone, and W_p is the non-essential (or plastic) work related to the outer plastic zone (Fig. 1b). W_e is a pure crack resistance parameter and essentially a surface energy. For a given specimen thickness, W_e is proportional to the ligament length l. W_p is a volume energy and is proportional to l^2 (also for a given specimen thickness). Thus the total fracture work W_f in Equation 2 can be rewritten as:

$$W_f = w_e Bl + \beta w_p Bl^2 \quad (3)$$

where w_e and w_p are the specific essential work of fracture and specific non-essential work, respectively. B is the specimen thickness and β is the shape factor. The specific total fracture work, w_f, is given by:

$$w_f = \left(\frac{W_f}{Bl}\right) = w_e + \beta w_p l. \quad (4)$$

Since both w_e and w_p are material constants, and β is independent of l, w_f will vary in a linear manner with l (Fig. 1c). By extrapolating the curve of $w_f - l$ to zero ligament length, w_e can be obtained. It has been proven theoretically and confirmed experimentally that the specific essential work of fracture (w_e) is equivalent to the critical J-integral value [17, 18].

2.3.3. Instrumented drop-weight dart impact test

For the instrumented drop-weight dart impact tests, the injection moulded plaques were cut into two halves, with the upper half (the half that is close to the injection gate) used for this part of the test programme. Each sample is having dimensions of $75 \times 80 \times 6$ mm^3. A total of ten samples were tested for each composition. A Ceast Fractovis instrumented drop-weight impact tester with a hemispherical tup (tip diameter = 20 mm) was used for the test. The impact speed was 10 m/s. The samples were fully clamped by an annular support-ring and movable clamp mechanism. The diameter of the support-ring and movable clamp were both equal to 38.1 mm.

2.4. Fractography

The fractured surfaces were examined by a Jeol (JSM-820) scanning electron microscope. The examined surfaces were coated with a thin layer of gold prior to SEM inspection.

3. Results and discussion

The average glass fibre length for the 0GF, 9GF, 17GF and 30GF hybrids are measured to be 0.22, 0.34, 0.26 and 0.27 mm respectively. It can be seen that except for the 9GF hybrid, the average fibre lengths for the other 3 hybrids are very close to each other.

Fig. 2 shows the notched Charpy impact strength against IM content for the blends and hybrids. The impact strength increased by approximately five-fold when the IM content increased from zero to 29.2 vol% in the former but little improvement is seen in the latter. Without the addition of the IM particles, the impact strength of 0GF was almost twice that of the PP

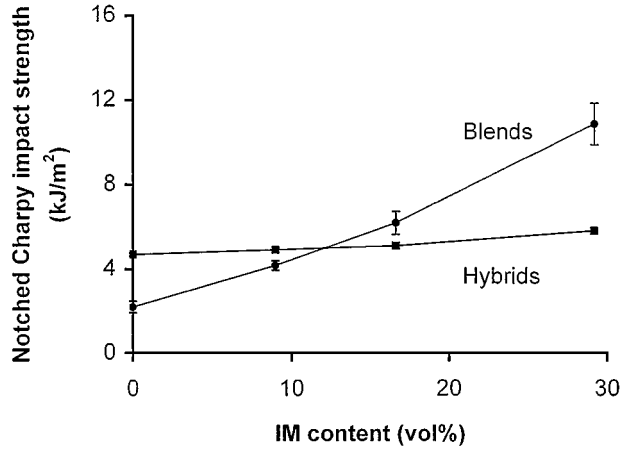

Figure 2 Notched Charpy impact strength against IM content for the blends and hybrids.

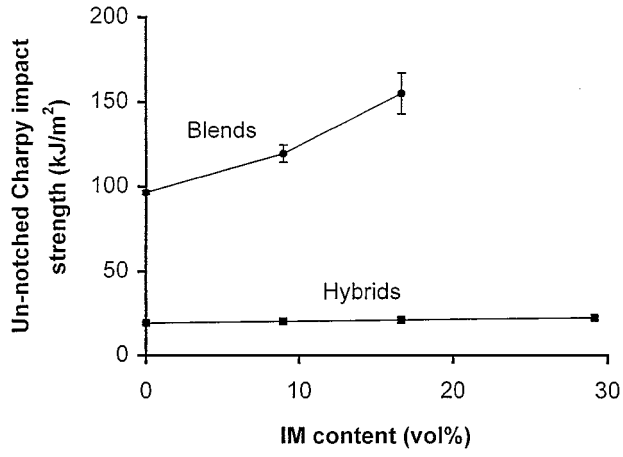

Figure 3 Un-notched Charpy impact strength against IM content for the blends and hybrids.

homopolymer. Even for the samples with 9.0 vol% of IM, the impact strengths of the hybrids are still higher than that of the blends. However, when the IM content was increased to over 16.6 vol%, the 17IM and 30IM samples absorbed more energy than their counterparts with the glass fibre addition.

In the un-notched Charpy impact tests (Fig. 3), there is a mark increase in the impact strength over the notched samples (see Fig. 2) for both blends and hybrids. It is believed that excessive energy was needed to initiate the crack in the un-notched samples. For the notched samples, crack initiation was much easier at the blunt notch tip. It is now clear that the impact resistance of the blends were much better than that of the hybrids over the whole IM content range studied (Fig. 3). In the hybrids, the glass fibre ends close to the bottom surface of the un-notched Charpy sample acted as sites of stress concentration from which cracks can be easily developed. The impact strength for the hybrids

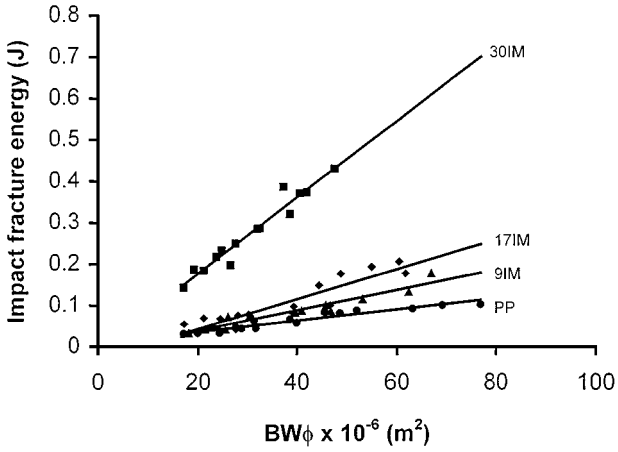

Figure 4 Plots of SENB impact energy U against $BW\phi$ for IM/PP blends with different IM content.

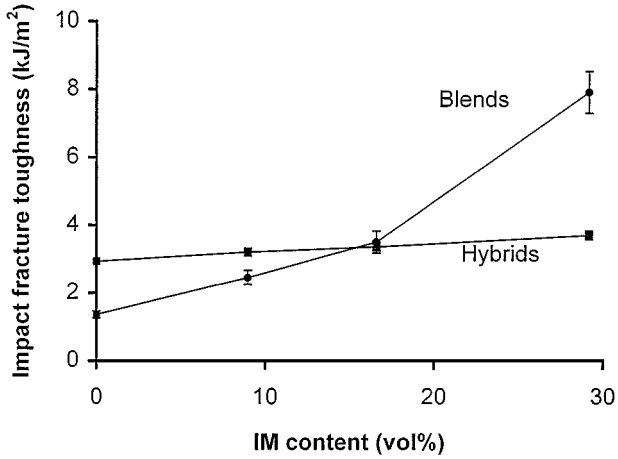

Figure 5 Impact fracture toughness of the blends (G_c) and hybrids (w_e) measured at an impact speed of 2 m/s.

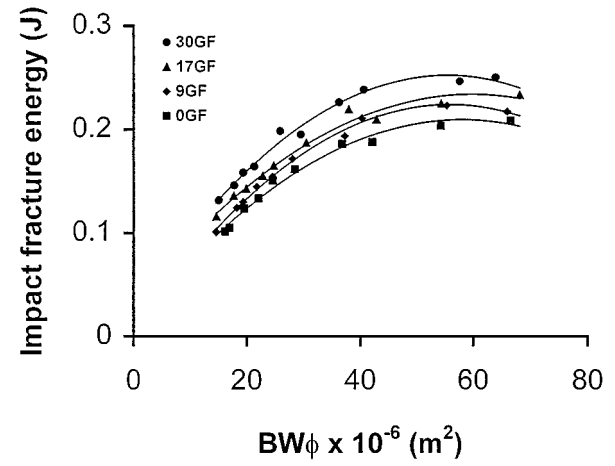

Figure 6 Plots of SENB impact energy U against $BW\phi$ for IM/GF/PP hybrids with different IM content.

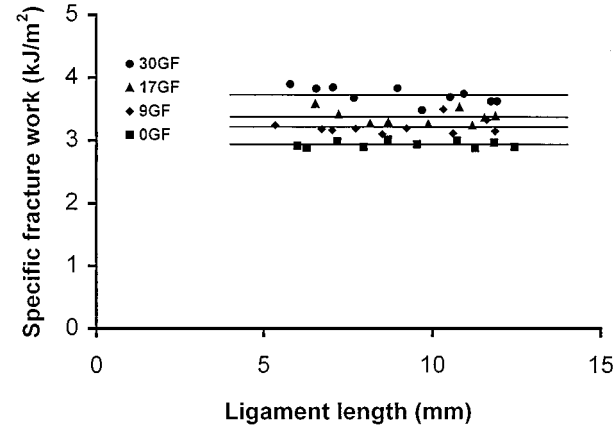

Figure 7 Specific fracture work against ligament length for IM/GF/PP hybrid composites.

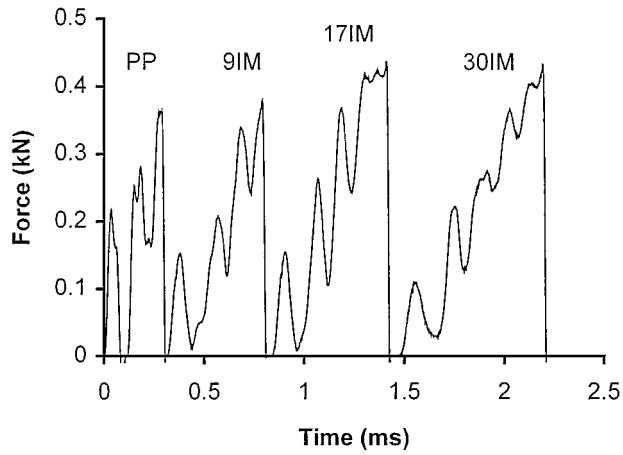

(a)

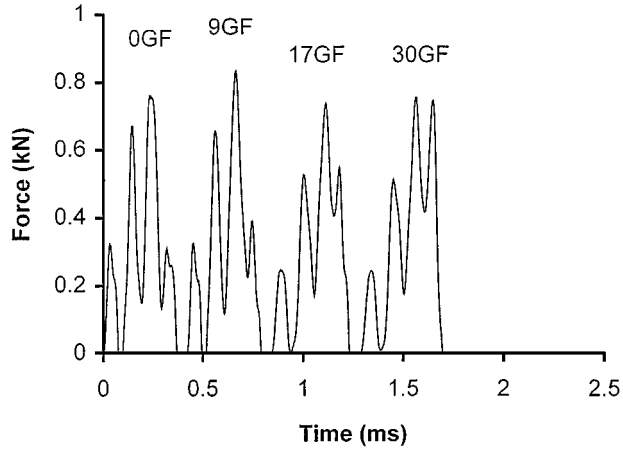

(b)

Figure 8 Typical impact force-times curves for the (a) IM/PP blends, and (b) IM/GF/PP hybrids with the SENB geometry.

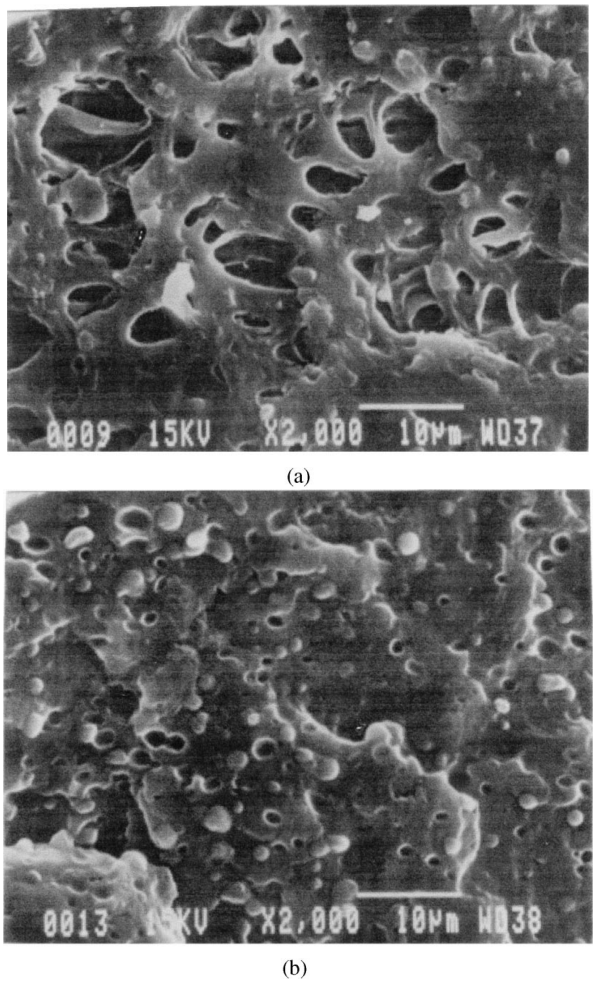

Figure 9 Impact fracture surface morphology for a SENB 30IM sample. (a) Region close to the initial crack tip; (b) Region far away from the initial crack tip.

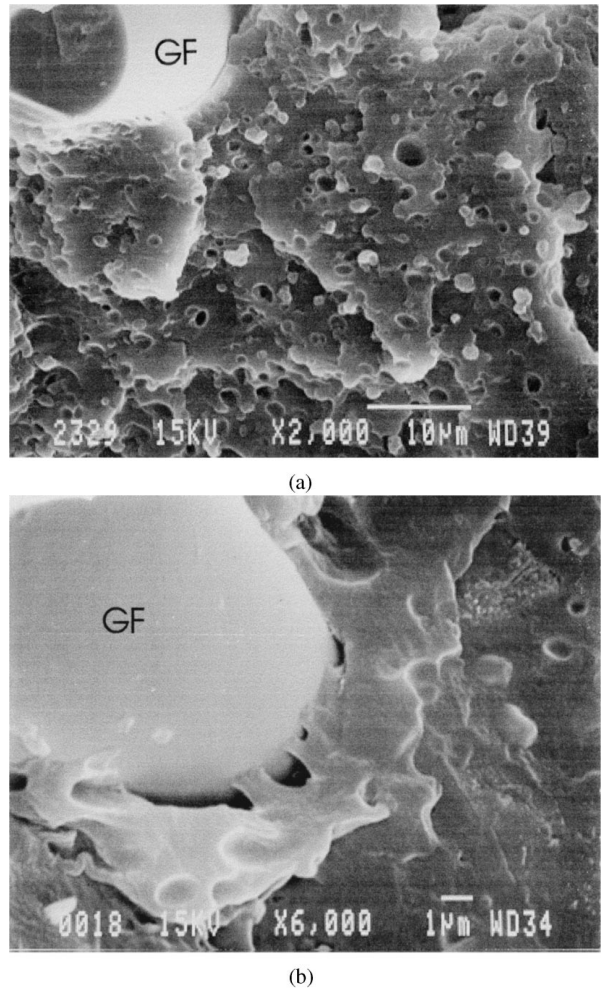

Figure 10 Impact surface for a SENB 30GF sample at regions close to the initial crack tip. (a) Cavitation of PP matrix around the IM particles was prohibited; (b) Glass fibre debonded from the PP matrix.

remained at around 20 kJ/m^2 regardless of the IM content, but increased with IM content for the blends. The un-notched Charpy impact strength for 30IM is not included in Fig. 3 because the samples cannot be broken in the impact tests.

For materials that fractured in a brittle manner under impact loading, the impact fracture toughness (G_C) can be measured from the slope of the U against $BW\phi$ plot (see Equation 1). The U against $BW\phi$ plot for the IM/PP blends containing different IM content are shown in Fig. 4. It is worth pointing out that both 17IM and 30IM samples failed in a semi-brittle manner, with corresponding stress-whitening zone ahead of the crack tips. Therefore crack tip plastic zone corrections have been carried out [13]. For PP and 9IM samples, no crack tip plastic zone correction was needed. The G_C for the blends as measured from the slope of the U against $BW\phi$ plot in Fig. 4 are shown in Fig. 5. Up to the 17% IM sample, there is a gradual increase in the G_C value, thereafter, a dramatic rise of approximately 250% (from the 17IM sample) is seen in the 30IM sample.

When U against $BW\phi$ plot was constructed for the IM/GF/PP hybrids, straight-line relationships were no longer observed (Fig. 6). Therefore the essential work of fracture [17, 18] approach was used (see Equation 4). When the total specific fracture work, w_f was plotted against the ligament length l, straight-line relationships were obtained for all the hybrids under investigation (Fig. 7). By extrapolating the straight lines to the Y-axis, the specific essential work of fracture, w_e, can be obtained, and are shown in Fig. 5 as a function of IM content. In contrary to the IM/PP blends, the effect of IM content on the IM/GF/PP hybrids was relatively mild. There was only a slight rise of 43% in w_e as the IM content increased to 29.2 vol%. We have to bear in

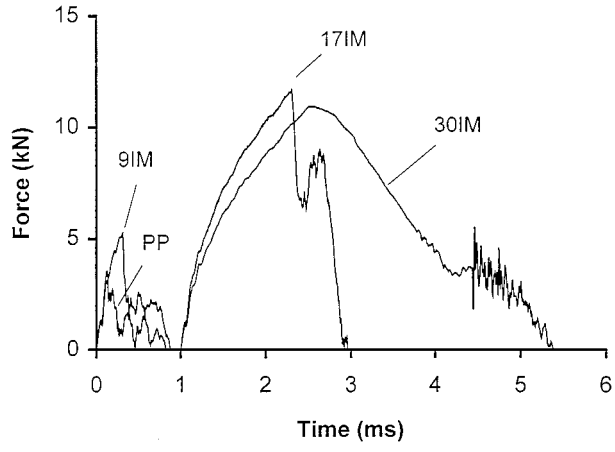

Figure 11 Impact force-times curves for the IM/PP blends measured from the drop weight dart impact test.

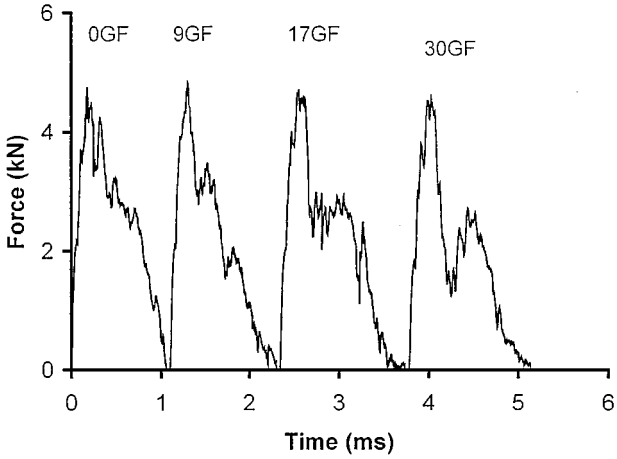

Figure 12 Impact force-times curves for the IM/GF/PP hybrids measured from the drop weight dart impact test.

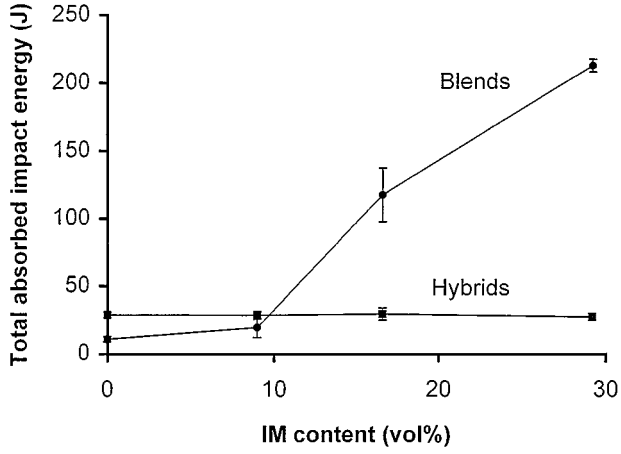

Figure 14 Total impact energy measured from the drop weight dart impact test.

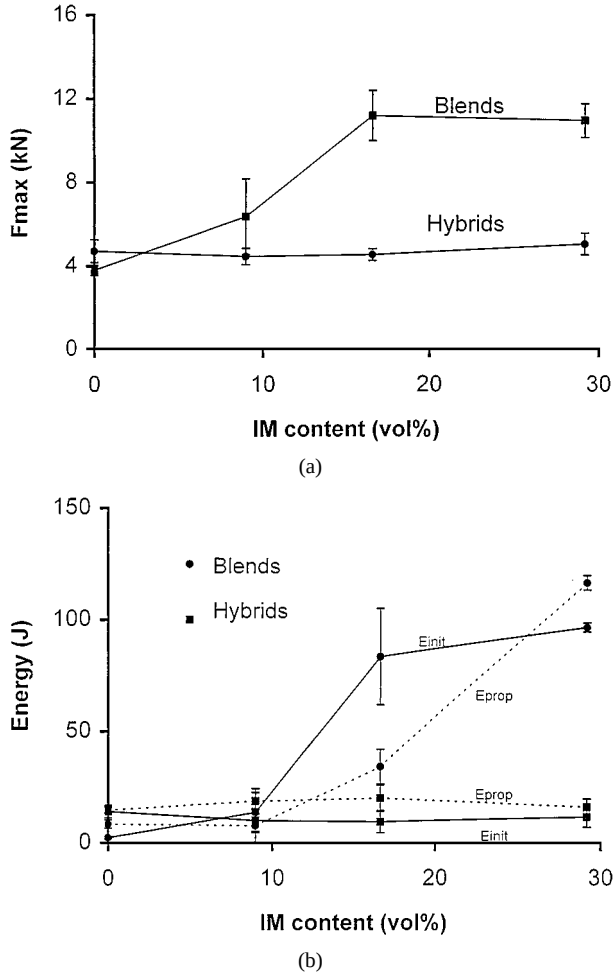

Figure 13 Drop weight dart impact test results: (a) F_{max}, and (b) E_{init} and E_{prop} against IM content.

mind that the IM contents in the hybrids were in fact higher than the quoted values when calculated with reference only to the PP matrix. This implies that the energy absorption mechanisms arise from the IM in the IM/GF/PP hybrids are not functioning as well as they do in the IM/PP blends.

On closer examination of Fig. 7, the following points were observed: (i) all the straight lines have slopes close to zero; and (ii) the value of w_f increased with IM content at any fixed ligament length. In relation to the zero gradients for the w_f vs. l plots, either the nonessential work term (w_p), or the shape factor β, or a combination of both, which are close to zero.

Typical impact force-time curves using the SENB specimen geometry for the blends and hybrids are shown in Figs 8a and b respectively. For the blends, it can be seen from Fig. 8a that irrespective of the IM content, the force-time curves dropped to zero instantaneously upon reaching the maximum force. This implied that nearly all the impact energy was involved in crack initiation. Once the crack was propagating, very little additional energy would be consumed. Therefore the theory of LEFM can be applied to the IM/PP blends.

For the hybrids (Fig. 8b), the impact force did not drop abruptly to zero from the maximum force. A substantial proportion of the impact energy was involved in the crack propagation stage. Therefore the theory of LEFM cannot be applied.

Impact fracture surface morphologies for a SENB 30IM blend sample are shown in Fig. 9. It can be seen that in regions close to the initial crack tip (Fig. 9a), the PP matrix was severely damaged by debonding followed by cavitation around the IM particles, which is the dominant energy absorption mechanism that took place in the crack initiation part of the force-time curves. In the fast crack propagation region of the fracture surface (Fig. 9b), cavitation of the PP matrix was absent.

Fig. 10 shows the impact fracture surface of a SENB 30GF hybrid sample at regions close to the initial crack tip. In Fig. 10a, it can be seen that cavitation of the PP matrix around the IM particles was prohibited (compare with Fig. 9a for the 30IM sample). A pull-out glass fibre (GF) is being shown on the upper left hand corner of the micrograph. Fig. 10b shows the debonding of a glass fibre from the surrounding PP matrix. From the relatively clean surface of the glass fibres, weak interfacial bondings can be inferred. The weak interfacial bonding can promote the energy dissipation mechanisms like debonding and fibre pull-out. And it is believed that they are the dominant energy absorption mechanisms for the hybrids.

In contrary to our present observation in Fig. 6, Hashemi and Mugan [19] have observed a linear relationship in the impact fracture energy (U) vs. $BW\phi$

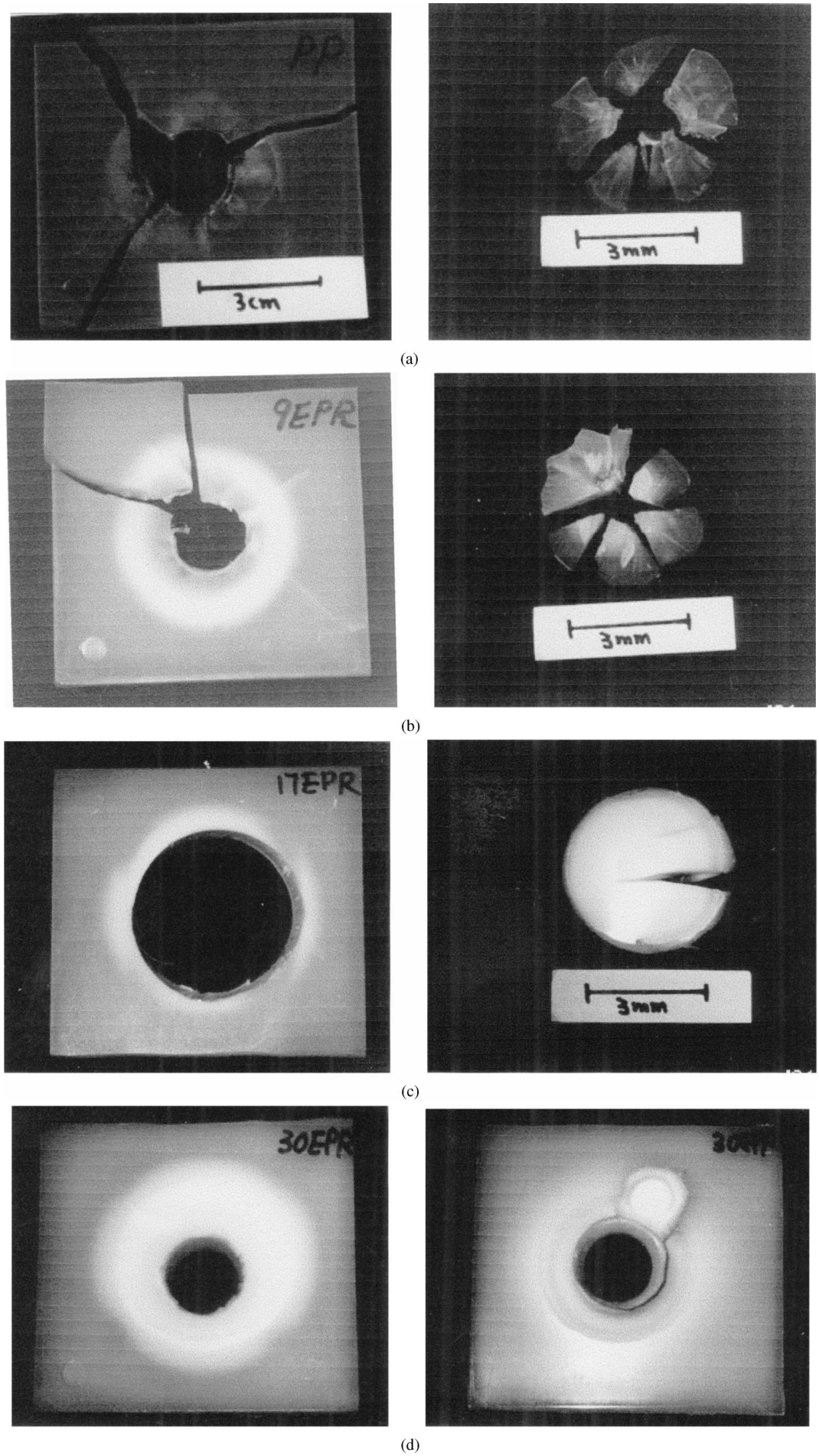

Figure 15 Drop weight dart impact fractured fragments of (a) PP; (b) 9IM; (c) 17IM and (d) 30IM.

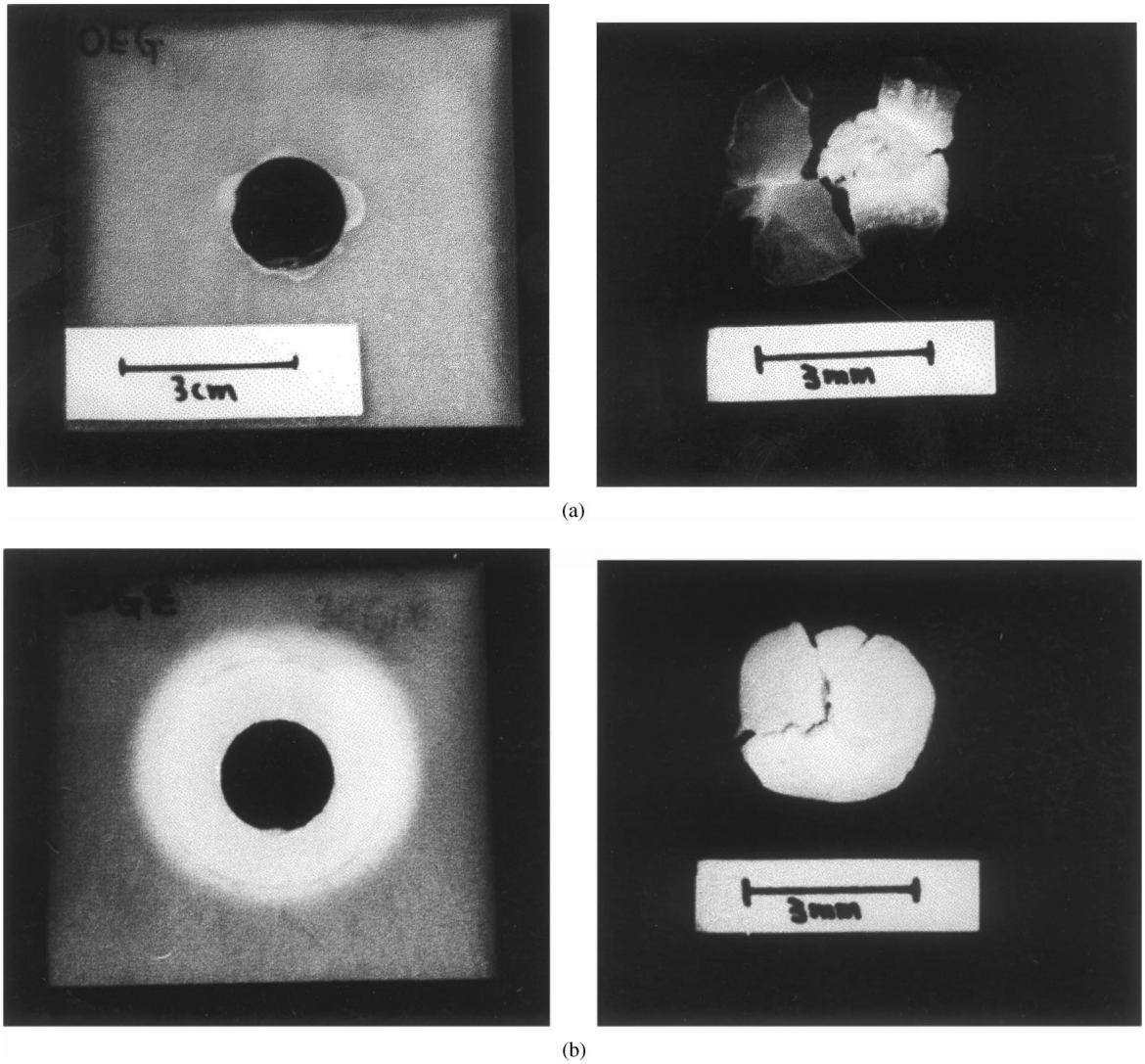

Figure 16 Drop weight dart impact fractured fragments of (a) 0GF and (b) 30GF.

plots for short glass fibre reinforced nylon 66. The possible cause for the non-linearity in Fig. 6 may be due to the difference in strength of the interfacial bonding. As mentioned above, the bonding between glass fibre and PP matrix is relatively weak in the present investigated hybrids (Fig. 10b). Therefore, fibre/matrix debonding may have taken place ahead of the crack tip. This is similar to the crack tip plastic yielding observed in ductile materials that contributes to the non-linearity in the U vs. $BW\phi$ plots. In our recent study on the impact fracture of short glass fibre reinforced nylon 66, a strong fibre/matrix bonding was observed. The impact fracture energy vs. $BW\phi$ plots are linear, which is similar to that observed in [19].

The drop weight dart impact force-time curves for the blends and hybrids are shown in Figs 11 and 12 respectively, from which very distinct characteristics can be observed between the two class of materials. For the blends, the overall force-time curves were highly dependent on the IM content. The impact duration increased with IM content for the blends, but were not affected for the hybrids. A comparison of the maximum force F_{max} against IM content for the blends and hybrids are shown in Fig. 13a, while initiation energy E_{init}, and propagation energy E_{prop} are shown in Fig. 13b. It can be seen that for the blends F_{max}, E_{init}, and E_{prop} are increased with IM content, but they remained relatively constant for the hybrids. The total impact energy, E_{total} $(= E_{init} + E_{prop})$ for both type of materials are shown in Fig. 14. For IM content $\leq$10 vol%, E_{total} for the hybrids were higher than the blends. When IM content $\geq$10 vol%, the reverse situation occurred.

Samples of dart impact fractured blend specimens are shown in Fig. 15. In Fig. 15a to c, the photographs on the left show the front surface of the impact fractured samples, while the photographs on the right show the central segmented fragments. In Fig. 15d, the front and back surfaces of an impact fractured 30IM sample were shown on the left and right respectively.

Both PP and 9IM samples failed in a similar manner (compare Fig. 15a and b), and hence having similar force-time curves (see Fig. 11). Unlike the previous two examples where the central pieces have been shattered, the 17IM samples failed in a totally different manner. The central circular piece is highly stress-whitened and contains a single radial crack, which was arrested at the clamping boundary (Fig. 15c).

In the case of the 30IM sample, the test plate remained in one piece after impact. A cup, in the shape

of the impact tup, was drawn out of the plate. A circular tear could be seen at the tip of this cup (Fig. 15d). The non-catastrophic failure highlighted the ductile nature of this polymer blend with the impact area being stretched significantly, before the tip was partially torn away from the main body.

Samples of dart impact fractured 0GF and 30GF hybrid specimens are shown in Fig. 16. The two types of sample failed in a similar manner and appeared to be brittle in nature. The major difference being that close to the damage region, stress whitening were observed in the 30GF samples but not in the 0GF samples. The behaviour for the 9GF and 17GF samples are similar to the 30GF samples.

4. Conclusions

The impact fracture behaviour of impact modifier modified PP (blends) and short glass fibre reinforced PP (hybrids) have been investigated. The impact fracture toughness of the blends can be measured from the G_C approach. For the hybrids, the impact fracture energy against $BW\phi$ relationship is highly nonlinear, with the result that the G_C approach cannot be applied. The essential work of fracture approach was found to be applicable to this class of materials.

Both impact fracture toughness (G_C for the blends and w_e for the hybrids) and notched Charpy impact strength agree with each other for the blends and hybrids under consideration. IM has a strong toughening effect for the blends, but the effect for the hybrids are very limited. SEM observation has identified debonding and cavitation of the PP matrix around the IM particles are the main energy dissipation mechanisms in the blends. In the hybrids, glass fibre debonding and pull out are the main energy dissipation mechanisms. Cavitation of the PP matrix around the IM particles is limited in the hybrids.

The instrumented drop weight dart impact force-time curves for the PP, 9IM, and all the hybrid materials are all similar. These are also reflected by the similar impact fractured fragments for the materials, which all show the formation of a number of radial cracks followed by the development of a circumferential crack. The fractures appeared to be brittle in nature. For the 17IM and 30IM specimens, the fractured fragments appeared to be ductile in nature and are supported by the force-time curves.

Acknowledgement

This work was supported by the City University of Hong Kong Strategic Research Grant Number 7000607. The first author was the recipient of a research studentship from the City University of Hong Kong during the course of this work.

References

1. S. C. TJONG, J. S. SHEN and R. K. Y. LI, *Polymer* **37** (1996) 2309.
2. *Idem.*, *Polym. Eng. Sci.* **36** (1996) 100.
3. D. E. SPAHR, K. FRIEDRICH, J. M. SCHULTZ and R. S. BAILEY, *J. Mater. Sci.* **25** (1990) 4427.
4. S. F. BUSH, F. YILMAZ and P. F. ZHANG, *Plast. Rubb. & Compos. Process. Appl.* **24** (1995) 139.
5. J. KARGER-KOCSIS, T. HARMIA and T. CZIGANY, *Comp. Sci. Technol.* **54** (1995) 287.
6. S. HASHEMI and M. KOOHGILANI, *Polym. Eng. Sci.* **35** (1995) 1124.
7. L. S. CHEN, Y. W. MAI and B. COTTERELL, *ibid.* **29** (1989) 505.
8. T. VU-KHANH, *J. Thermoplastic Compos. Mater.* **4** (1991) 46.
9. P. H. TH. VOLLENBERG and D. HEIKENS, *J. Mater. Sci.* **25** (1990) 3089.
10. J. KARGER-KOCSIS, *Polymer* **20** (1979) 37.
11. J. KARGER-KOCSIS and V. N. KULEZNEV, *ibid.* **23** (1982) 699.
12. C. J. CHOU, K. VIJAYAN, D. KIRBY, A. HITTNER and E. BAER, *J. Mater. Sci.* **23** (1988) 2521.
13. W. Y. TAM, T. CHEUNG and R. K. Y. LI, *Polymer Testing* **15** (1996) 363.
14. S. V. NAIR, M. L. SHIAO and P. D. GARRETT, *J. Mater. Sci.* **27** (1992) 1085.
15. W. Y. CHIANG, W. D. YANG and B. PUKANSZKY, *Polym. Eng. Sci.* **32** (1992) 641.
16. J. G. WILLIAMS, "Fracture Mechanics of Polymers" (Ellis Harwood, Chichester, 1984).
17. J. S. WU, Y. W. MAI and B. COTTERELL, *J. Mater. Sci.* **28** (1993) 3373.
18. J. S. WU and Y. W. MAI, *Polym. Eng. Sci.* **36** (1996) 2275.
19. S. HASHEMI and J. MUGAN, *J. Mater. Sci.* **28** (1993) 3983.

Received 21 July 1997
and accepted 28 September 1999